

High Contrast Imaging with Spitzer : Constraining the Frequency of Giant Planets out to 1000 AU separations.

Stephen Durkan¹, Markus Janson², Joseph C. Carson³

ABSTRACT

We report results of a re-analysis of archival Spitzer IRAC direct imaging surveys encompassing a variety of nearby stars. Our sample is generated from the combined observations of 73 young stars (median age, distance, spectral type = 85 Myr, 23.3 pc, G5) and 48 known exoplanet host stars with unconstrained ages (median distance, spectral type = 22.6 pc, G5). While the small size of Spitzer provides a lower resolution than 8m-class AO-assisted ground based telescopes, which have been used for constraining the frequency of 0.5 - 13 M_J planets at separations of $10 - 10^2$ AU, its exquisite infrared sensitivity provides the ability to place unmatched constraints on the planetary populations at wider separations. Here we apply sophisticated high-contrast techniques to our sample in order to remove the stellar PSF and open up sensitivity to planetary mass companions down to $5''$ separations. This enables sensitivity to 0.5 - 13 M_J planets at physical separations on the order of $10^2 - 10^3$ AU, allowing us to probe a parameter space which has not previously been systematically explored to any similar degree of sensitivity. Based on a colour and proper motion analysis we do not record any planetary detections. Exploiting this enhanced survey sensitivity, employing Monte Carlo simulations with a Bayesian approach, and assuming a mass distribution of $dn/dm \propto m^{-1.31}$, we constrain (at 95% confidence) a population of 0.5 - 13 M_J planets at separations of 100 - 1000 AU with an upper frequency limit of 9%.

Subject headings: planetary systems - techniques: image processing - infrared: planetary systems

1. Introduction

The plethora of confirmed exoplanets to date is dominated by a population of planets within 5 – 6 AU of their host star. This has been due to the success of large-scale radial-velocity (Butler et al. 1996; Vogt et al. 2000; Mayor et al. 2003) and transit surveys (Pollacco et al. 2006; Baglin et al. 2009; Koch et al. 2010), which are biased to short separation planets and whose typical duration limit their ability to detect periodicities on the order of 10's of years. Such surveys account for a combined detection of ~ 1900 planets (See <http://exoplanet.eu> and <http://exoplanetarchive.ipac.caltech.edu/>), > 90% of

the entire exoplanet population. This sample enables statistically significant trends to be uncovered between planetary / host star properties and planet frequency, which in turn allows for planet formation and evolution theories to be stringently tested and constrained. However formation scenarios and evolutionary paths for wide giant planets with separations $\gg 5 - 6$ AU continue to prove challenging to constrain. This is due to a lack of systematic explorations by surveys with a sufficient degree of sensitivity and statistically robust population analyses.

Direct imaging provides the most viable technique to probe for giant planets at such wide separations. Extensive work has been carried out to expand the sample of wide giant planets through detection in large-scale direct imaging surveys (Masciadri et al. 2005; Biller et al. 2007; Lafrenière et al. 2007b; Kasper et al. 2007; Chauvin et al. 2010; Lecote et al. 2010; Ehrenreich et al. 2010; Carson et al. 2011; Janson et al. 2011; Vigan et al. 2012; Delorme et al. 2012; Biller et al. 2013; Chauvin et al. 2015). Whilst these surveys typically record non-

¹Astrophysics Research Centre, School of Mathematics & Physics, Queen's University, Belfast BT7 1NN, UK; sdurkan01@qub.ac.uk

²Department of Astronomy, Stockholm University, 106 91 Stockholm, Sweden

³Department of Physics and Astronomy, College of Charleston, Charleston, SC 29424, USA

detections, several planetary mass wide companions have been found, indicating that although these types of planets may be rare (Nielsen & Close 2010), they do exist with some frequency throughout the galaxy. By subjecting these imaging surveys to statistical analysis, an upper limit on this frequency can be determined. Concurring frequency upper limits have been found for wide giant planets over a separation range on the order of $10^1 - 10^2$ AU, corresponding to the parameter space at which observations are sensitive to Jupiter mass companions. These limits are shown in Table 1.

Sensitivity is confined to this range due to instrumental limitations. Imaging surveys typically favour the use of adaptive optics (AO) corrected instruments on 8m class ground based telescopes. The high angular resolution afforded by such instruments provides sensitivity to planetary mass companions at small separations, down to the order of 10 AU, inside of which the required contrast becomes unachievable as one approaches the core of the near diffraction limited point spread function (PSF). The outer sensitivity limit stems from anisoplanatism, where AO delivers poor wave front correction at increasing separation due to the different propagation paths and hence varying wave front distortion experienced by off-axis light. This substandard correction results in a decrease in image quality and therefore a reduction in sensitivity at large separations. Typical values for the isoplanatic angle, where distortion is statistically uniform allowing for good AO correction, are $10'' - 20''$ in the near infrared (NIR) (Sandler et al. 1994; Fritz et al. 2010), and thus imaging instruments are typically restricted to this field of view (FOV). This has severely limited sensitivity to planetary mass companions at separations beyond the order of 10^2 AU, for typical nearby targets.

Conducting imaging surveys from space based telescopes would negate this effect, however their small aperture diameters produce large diffraction limited PSF's, severely limiting their application for direct imaging of planets. Still, Marengo et al. (2006, 2009) have shown that the Spitzer space telescope is capable of sensitivity to planetary mass companions at large angular separations, within the background noise limited regime, with their studies of ϵ Eri and Fomalhaut. Recent studies of Vega, Fomalhaut and ϵ Eri by Janson et al. (2012, 2015) have demonstrated that sensitivity to planetary mass companions is achievable with Spitzer within the PSF noise-limited regime, with the application of sophisticated high-contrast reduc-

tion techniques.

Therefore we implemented a sophisticated PSF subtraction technique to enhance the sensitivity of archival Spitzer imaging surveys, enabling sensitivity to planetary mass companions over a separation on the order of $10^2 - 10^3$ AU. This parameter space has not previously been systematically explored by surveys to a sufficient degree of sensitivity, leaving the population of giant planets at these separations poorly constrained.

While the formation and origin of such wide orbit giants proves difficult to explain, their existence has been confirmed with the detection of several planetary mass companions e.g. 1RXS J1609-2105 b; 330 AU (Lafrenière et al. 2010), FW Tau b; 330 AU (Kraus et al. 2014a), HD106906 b; 650 AU (Bailey et al. 2014), GU Psc b; 2000 AU (Naud et al. 2014). Whilst core accretion and gravitational instability modes cannot readily explain the formation of such planets in situ (Ida & Lin 2004; Boss 2006; Rafikov 2007; Dodson-Robinson et al. 2009), and disk interactions cannot viably migrate planets out to $\sim 10^3$ AU, beyond the typical confines of the disk (Isella et al. 2009), several theories have been developed in an attempt to account for planetary existence at these large orbital separations.

One suggestion is that such a planetary system could be the result of dynamical capture of free-floating planets during dispersal of a stellar cluster. Simulations found this capable of producing planets at separations of > 50 AU (Parker & Quanz 2012) and $10^2 - 10^5$ AU (Perets & Kouwenhoven 2012). As an alternative, planet-planet scattering, in which multiple planets gravitationally interact after disk dissipation, can result in dynamical scattering of a planet out to wide separations on the order of 100's of AU (Rasio & Ford 1996; Veras & Armitage 2004; Chatterjee et al. 2008; Jurić & Tremaine 2008). Dynamical simulations by Veras et al. (2009) show these interactions capable of scattering giant planets out to separations of $10^2 - 10^5$ AU. However they find the population of planets that eventually end up in unbound orbits passing through these wide separations to be larger than the population on stable orbits. The total population of wide giant planets then decreases on timescales of ~ 10 Myr to produce a significantly depleted population at ages > 50 Myr where the majority of planets have been ejected from the system.

Constraining the population of giant planets at separations of $10^2 - 10^3$ AU is essential for assessing the

Table 1: Planet Frequency Upper Limits

Mass Range (M_J)	Separation Range (AU)	Planet Frequency	
		Fractional Upper Limit	Study
0.5 - 13.0	50 - 250	0.093	(Lafrenière et al. 2007b)
0.5 - 13.0	25 - 100	0.110	(Lafrenière et al. 2007b)
1.0 - 20.0	10 - 150	0.060	(Biller et al. 2013)
1.0 - 13.0	20 - 150	0.100	(Chauvin et al. 2010)

relevance of these theories, and allowing for stringent constraints to be placed on formation and evolution modes out to 1000's of AU.

2. Target Sample

Our target list is compiled from archival Spitzer data based on proximity and youth. Such targets prove favourable to imaging searches for planetary companions as young giant planets are intrinsically bright in the near infrared due to heat retention from formation. This brightness decreases as the planet ages and the heat dissipates (Baraffe et al. 2003; Burrows et al. 2003; Fortney et al. 2008). Younger targets therefore provide imaging sensitivity to a greater range of companion masses for a given detection threshold, compared to relatively older stars, allowing for detection of lower mass planets. Stars within close proximity to Earth provide sensitivity to companions over a greater range of physical separations for a given detection threshold at a specific angular separation, compared to a relatively distant target, allowing for detection of shorter period planets for a given mass sensitivity.

This motivates our choice of stars from the archival Spitzer program 34 (P34) for enhanced imaging analysis. This program targeted 73 nearby (< 30 pc), young stars and therefore provides an ideal basis for the sample of targets chosen here. Multiple age indicators including X-ray luminosity, chromospheric activity, Lithium abundance, rotation and photometric colour were originally used to select targets for P34 with ages below 120 Myr. We find these age estimates to be overly optimistic. Using a number of sources (e.g. Montes et al. 2001b; Zuckerman & Song 2004; Torres et al. 2008; Maldonado et al. 2010; Malo et al. 2013), we identify 55 of these targets to be members of young moving groups (YMGs) and place conservative age limits on the targets corresponding to reliable age estimates of YMGs taken from the literature; these age estimates are given in Table 2. We then place conser-

vative age limits on the remaining targets combining literature age estimates encompassing several techniques (e.g. Barnes 2007; Mamajek & Hillenbrand 2008; Plavchan et al. 2009; Tetzlaff et al. 2011; Vican 2012). The median target age is 85 Myr, although age limits range from 8 to 1050 Myr. The exception to this is HD 124498. Malo et al. (2013) identifies this target as a probable member of the β Pictoris YMG. However Chauvin et al. (2010) use several age dating techniques to reclassify HD 124498 as an older system with an age ≥ 100 Myr. We therefore place an age of 12 Myr - 10 Gyr on HD 124498 to ensure any statistics encompassing age estimations produce conservative results. The median target distance, spectral type and H band magnitude are 23.3 pc, G5 and 5.289 respectively.

We choose an additional archival Spitzer program to add to our target sample, program 48 (P48). This program targeted 48 nearby (< 35 pc) stars with known planetary companions, discovered via radial velocity. As such, these planets are on relatively short orbits, spanning a parameter space currently inaccessible to direct imaging techniques. These exoplanet host stars are relatively old and no confident age limits can be found for the majority of the sample throughout the literature. For consistency, and to justify that any derived statistical result represents a conservative limit, we adopt a conservative age of 1 Gyr - 10 Gyr for all P48 stars. This age range spans the breadth of poorly constrained literature ages for the majority of the sample. The exceptions to this are HD 13507, HD 1237 and AF Hor, which are identified as members of YMGs with independent literature age estimates that support the association membership. Whilst these targets may prove unfavourable to a deep imaging study, due to their extended ages, the strength in their addition to the sample is that they provide an additional 48 references to aid in PSF reduction of the 73 P34 stars, contributing to an increase in achievable contrast and sensitivity to smaller mass companions. P48 was executed under the exact observational parameters as P34.

Table 2: Moving Group Age Estimates

YMG	Age Estimate (Myr)	Age Reference
Local Association (LA)	20 - 150	(Montes et al. 2001b; Brandt et al. 2014)
β Pictoris	12 - 22	(Malo et al. 2013)
Ursa Major	400 - 600	(King et al. 2003)
Castor	100 - 300	(Barrado y Navascues 1998; Montes et al. 2001b)
IC2391	45 - 55	(Stauffer et al. 1997)
Hyades	575 - 675	(Perryman et al. 1998)
Her-Lyr	211- 303	(Eisenbeiss et al. 2013)
AB Dor	70 - 120	(Malo et al. 2013)
Octans-Near	30 - 100	(Zuckerman et al. 2013)
Argus	30 - 50	(Malo et al. 2013)
TW Hydrae	8 - 12	(Malo et al. 2013)
Tuc-Hor/Columba/Carina	20 - 40	(Malo et al. 2013)

Along with P48 encompassing a similar spectral sample of stars as P34, median spectral type and H band magnitude G5 and 4.957 respectively, this ensures P48 targets provide sufficient P34 PSF references. The median distance of P48 stars is 22.6 pc. So whilst the age range of P48 stars limit sensitivity to low mass planets, their proximity ensures sensitivity to larger mass planets over a wide range of separations. Therefore their inclusion our sample for reduction and analysis as well as providing additional references is justified. However we note the potential bias introduced to any population constraint statistically derived from a deep imaging search encompassing a sample of stars hosting short period planets. If we consider planet-planet scattering to be a relevant mechanism for giant planet production at $10^2 - 10^3$ AU separations, the presence of a detected planet at a separation comparable to where a wide giant planet is expected to initially form, incorporates some degree of bias into our statistics that we cannot quantitatively evaluate. Therefore we do not correct for this possible bias. The combined target properties are given in Table 3.

3. Observations and Data Reduction

The combined 121 targets were observed with the Infrared Array Camera (IRAC; Fazio et al. 2004) on the Spitzer Space telescope (Werner et al. 2004) under archival programs 34 and 48 between 2003 and 2004, during the cryogenic phase of the Spitzer mission. Images were obtained simultaneously at 3.6, 4.5, 5.8 and 8 μ m (channels 1 - 4 respectively). We choose Channel 2 as the primary channel to analyse based on evolutionary model predictions that planetary mass companions

are at their peak luminosity within the 4.5 μ m band (Barrafe et al. 2003). Therefore this channel offers the best sensitivity for planet detection. We also analyse IRAC channel 1 images as a means to vet potential companions.

All targets were observed with a 30s frame time allowing for an effective exposure time of 26.8s per dither position. Each observation was carried out with a five-position Gaussian dither pattern. The Spitzer Science Center (SSC) IRAC Pipeline (version S18.25.0) performed data reduction for all observations, producing basic calibrated data (BCD) frames. This pipeline also produced corrected BCDs (CBCD) where saturated point sources have been fitted with unsaturated point sources by fitting an appropriate PSF that is matched to the unsaturated wings of the source. A final post basic calibrated data (PBCD) frame is then created by mosaicking the relevant CBCD frames at each dither position to produce a sub-pixelated image with a 0.6'' per pixel resolution and a 5.2' x 5.2' FOV. Such saturation corrected images are unsuitable for a close companion search as pixels towards the PSF core may have been replaced with model pixel values, ensuring that any information about potential companion sources at these separations is lost. However we favour the use of PBCD's over BCD's due to the additional artifact correction performed on the former by the SSC IRAC pipeline. Therefore we generate a composite frame consisting of a PBCD image where saturation corrected regions, identified in the relevant mask files, have been replaced with pixel values generated from mosaicking the relevant BCD frames. These pixel values have been sub-pixelated to the equivalent 0.6'' per pixel resolution. Figure 1 shows an example

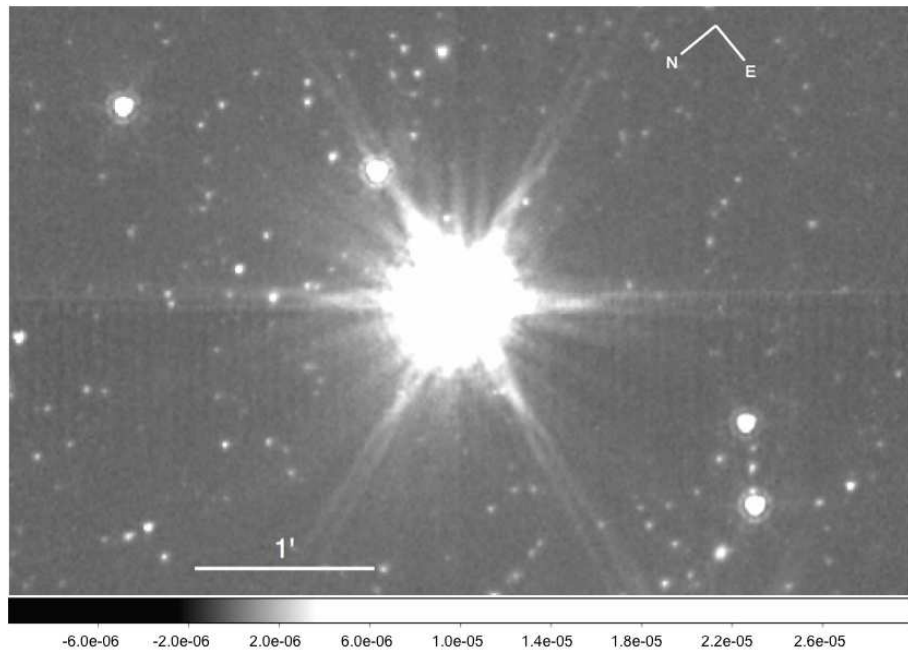


Fig. 1.— Example of a composite PBCD / BCD $4.5 \mu\text{m}$ image of HD 217813, displaying the extent of the PSF and Spitzer spider features. The wide FOV reveals a multitude of point sources which must be vetted for planet candidacy. HD 217813 properties lie close to the median of the sample, H mag = 5.232, G5V star at 24.7pc.

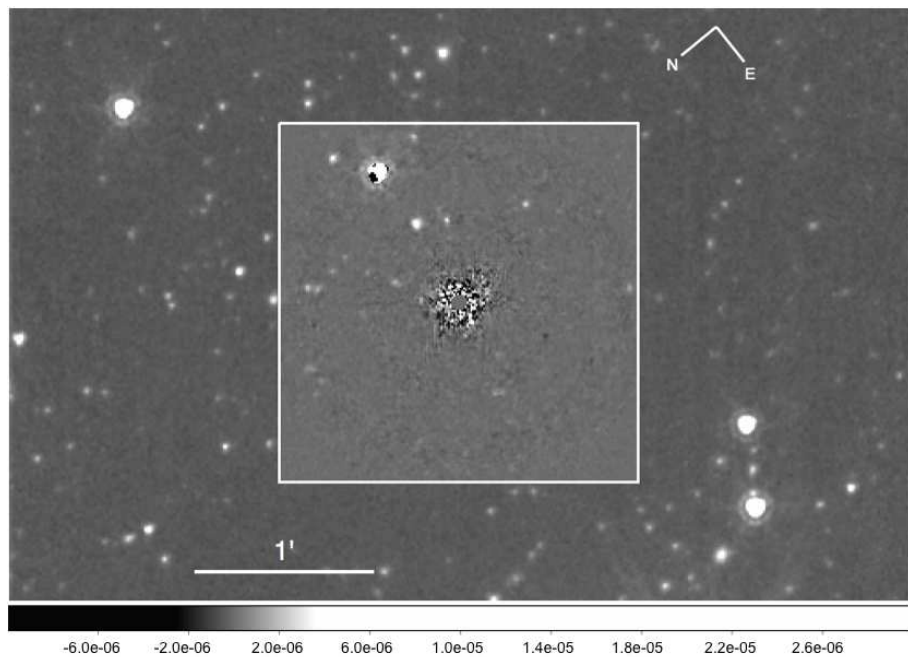


Fig. 2.— Final reduced image of HD 217813 depicting the same FOV as Figure 1. The white box highlights the $2.01' \times 2.01'$ PCA optimization region. Regular PSF subtraction of a mean stack image has been performed outside the optimisation region.

of such a composite PBCD / BCD image.

3.1. PSF Subtraction

We calculate the centre of each target PSF by the fitting of a 2 dimensional Gaussian, the centre of each image is then shifted to this position. Each image is then normalised by the central brightness of the stellar PSF, estimated from the saturation corrected images. This provides an image stack of target PSF's that have similar normalised flux values. We then mask the saturated cores of each image for subsequent image reduction. Each individual image is then robustly centred with respect to the stack by subtraction of a median stack image over a range of sub-pixel offsets. The offset producing the minimum residuals is then used to align each image. The image stack constitutes the library of PSF's used to construct a reference PSF for image subtraction. This accurate alignment of target PSF's then provides better performance of any reference construction, ultimately leading to improved sensitivity in any final reduced image.

Here we use Principal Component Analysis (PCA) to construct the optimal reference PSF to subtract from the target PSF. Variations of PCA such as PynPoint (Amara & Quanz 2012) and KLIP (Soummer et al. 2012) have the same underlying principle; a linear combination of orthogonal basis sets are used for reference construction. These basis sets represent the decomposition of the reference library into its principal components. The linear coefficients are then generated by the projection of the target onto each individual basis. PCA performed here follows a KLIP-based analysis.

We limit the PCA optimization to a 201 x 201 pixel sub-section of each 3.6 μm and 4.5 μm image, centred on the star. This corresponds to 2.01' x 2.01' FOV. This reduced area is chosen as a favourable trade off between algorithm efficiency and sensitivity to wide separations, with 2.01' corresponding to separations on the order of 10^3 AU, at the typical target distance. PCA is performed on concentric annuli centred on the star. The radii of the annuli are chosen such that each annulus contains 1500 pixels. Reference annuli containing astronomical sources such as background stars, stellar companions or surviving bad pixels are excluded to prevent the algorithm from subtracting any true planetary PSF, and to prevent any fake planetary signal being injected into the final image. Since flux increases towards the PSF core, the larger flux val-

ues towards the inner region of each annulus dominate the weighting of the orthogonal basis. This may produce the lowest residuals but the outer annular regions will have experienced a substandard reduction. By performing PCA four times on each target and increasing the radius of the inner saturation mask, and therefore shifting the radii of the 1500 pixel annuli, we ensure that each section of the frame has been encompassed by an inner annular region and experienced a full quality reduction. The final images to be analysed are then composites of these four separate PCA reduced frames whose constituent parts have experienced optimal reduction. A final PCA reduced image can be seen in Figure 2.

PCA reduction is typically performed at neighbouring states of the telescope / instrument system and provides optimal PSF subtraction when carried out in tandem with angular differential imaging application, where the PSF remains quasi-static over the observation. Here we apply PCA to a sample observed at varying states of the telescope / instrument system taken over the course of one year, e.g. varying stellar magnitude, spectral type, telescope roll angle. Therefore, our study constitutes a trial of PCA on an unfavourable data set, testing its effectiveness at the limits of its application. Similar conditions are required for optimal PSF subtraction using LOCI (Lafrenière et al. 2007a) and thus we favour PCA for its speed enhancement.

3.2. Image Sensitivity & Companion Identification

We evaluate the sensitivity in the final PCA reduced images at 5σ detection limits by relating the standard deviation in concentric 1 pixel width annuli centred on the star, to the zero-point flux of Vega using the method of Marengo et al. (2009). This generates sensitivity values in units of Vega magnitudes. As any potential companion will suffer from partial flux subtraction during the PCA reduction, we must account for the throughput of sources in the sensitivity estimation. We inject synthetic companions into each target image at position angles 0° and 90° so as to cover spider and non-spider regions, at five pixel intervals out to the edge of the optimisation region, and estimate throughput after PCA application. The mean throughput is then calculated at each separation and linearly interpolated to produce throughput values for each pixel separation, consistent with sensitivity estimation in one-pixel width annuli. The mean throughput over the image stack is then used for sensitivity estimation.

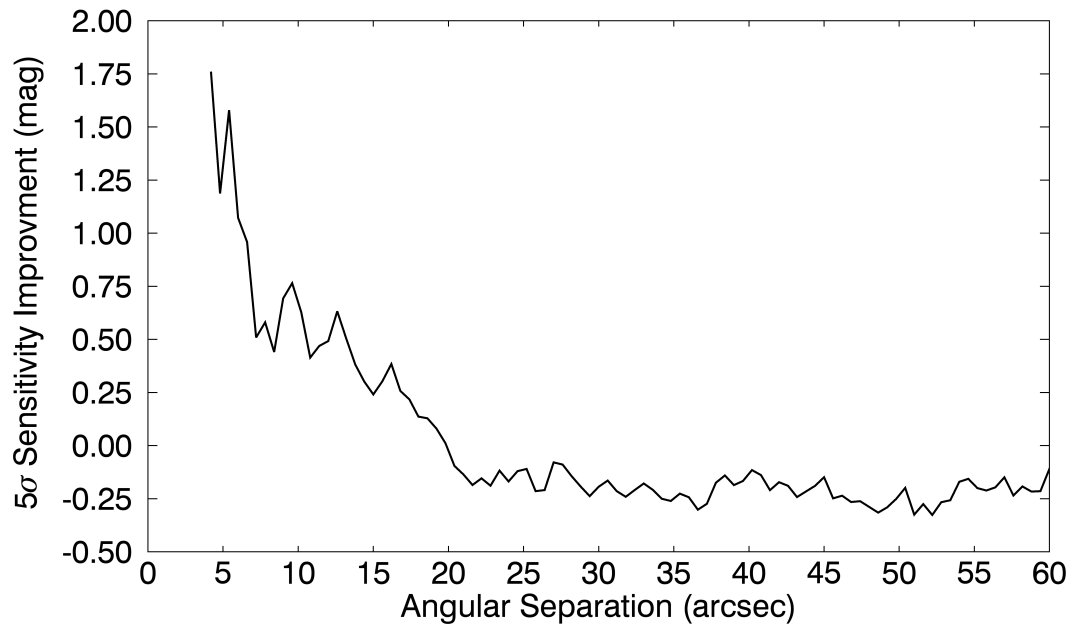


Fig. 3.— PCA sensitivity improvement with respect to conventional PSF subtraction, as a function of separation. The decrease in improvement around $20''$ corresponds to the transition between the PSF noise-limited regime and the background noise limited regime. The jagged nature of the curve stems from preferential reduction of inner annulus regions.

We evaluate the performance of the PCA reduction by computing sensitivity curves for both PCA optimized and conventional PSF subtracted images (i.e., subtraction of a mean stack image) and calculating the sensitivity improvement provided by PCA for each target. The median sensitivity improvement curve is then generated. This curve, displayed in Figure 3, shows that PCA offers superior image sensitivity at separations less than $20''$, within the PSF noise-limited regime, and provides a median improvement of ~ 0.9 magnitudes at separations less than $10''$. This validates the application of PCA in a study encompassing a diverse sample of stars, observed at varying states of the telescope / instrument system. The ~ 0.9 magnitude improvement in the contrast limited regime demonstrates the relevance of applying and developing sophisticated high-contrast techniques to archival Spitzer data, where we have enhanced sensitivity to planetary mass companions at relatively small angular separations. This allows for the possibility of subsequent planet detection within a previously elusive parameter space and enabling more stringent constraints to be placed on the wide giant population. In the background noise limited regime, separations greater than $20''$, PCA does not provide any sensitivity improvement over regular PSF subtraction. This is due to the random nature of background noise which PCA cannot reference.

We use two initial criteria to identify potential planetary mass companions. Firstly each $4.5 \mu\text{m}$ reduced image is visually inspected to identify realistic PSF shapes, allowing real sources to be distinguished from potential surviving bad pixels. Any realistic PSF is then vetted for planetary candidacy by comparison of the $4.5 \mu\text{m}$ and $3.6 \mu\text{m}$ images. The spectral energy distribution of a non-irradiated 0.5 - 13 Jupiter mass companion, at the typical ages of our sample, is such that planetary flux at $3.6 \mu\text{m}$ is typically > 1 magnitude fainter than at $4.5 \mu\text{m}$ where peak emission occurs (Baraffe et al. 2003; Spiegel & Burrows 2012). In contrast to a background star, which is expected to be approximately equally bright in the $3.6 \mu\text{m}$ and $4.5 \mu\text{m}$ images, a planet detection recorded around the 5σ limit at $4.5 \mu\text{m}$ is not expected to be recovered to any reasonable significance at $3.6 \mu\text{m}$. This allows planetary sources to be distinguished from faint background stars without the need for a proper motion analysis. Therefore we look for source non-detection at $3.6 \mu\text{m}$ to confirm planet candidacy.

4. Results

4.1. Observational Sensitivities

Figures 4 and 5 show the $4.5 \mu\text{m}$ median sensitivity curves for the P34 and P48 stars respectively. Within $\sim 20''$ sensitivity decreases towards the PSF core where the residual PSF noise exhibits the largest variance, limiting sensitivity to lower magnitude companions. Outside $\sim 20''$ PCA provides no sensitivity improvement and we are limited by background noise which tends to be constant, thus magnitude sensitivity at these separations is roughly constant. Figures 4 and 5 also map sensitivity as a function of projected physical separation out to ~ 1400 AU at the median distance of P34 and P48 stars, 23.3 pc and 22.6 pc respectively. P34 and P48 stars provide comparative magnitude sensitivity limits.

These magnitude sensitivity limits can be translated into mass sensitivities using mass-luminosity evolutionary models. One caveat is the discrepancy between hot- (Chabrier et al. 2000; Baraffe et al. 2003; Burrows et al. 2003) and cold-start (Marley et al. 2007; Fortney et al. 2008) models, where the later predict much fainter planets at young ages. Here we will consider hot-start models which are consistent with existing observational data (Janson et al. 2011). However it can be noted that the models converge on the order of 10's of Myrs for low mass planetary companions ($\leq 2M_J$) and on the order of 100's of Myr for higher mass planetary companions (Spiegel & Burrows 2012). Thus our choice of model will not lead to significant disparity in mass sensitivity over the complete sample at the typical ages considered. COND-based models (Allard et al. 2001; Baraffe et al. 2003), applicable for companion temperatures below 1700K, which is a relevant temperature range for 0.5 - 13 M_J companions at the sample ages, are used here.

The corresponding mass sensitivities for the median P34 and P48 magnitude sensitivities are shown in Figures 4 and 5. With P34 targets, sensitivity down to $\leq 2M_J$ companions is achieved down to $\sim 5''$, corresponding to ~ 100 AU projected separation, whilst sensitivity down to $0.5 M_J$ companions is achieved for separations $\gtrsim 15''$ ($\gtrsim 350$ AU). Whilst P34 and P48 stars provide comparative magnitude sensitivity limits, the extended ages of P48 stars ensure an equivalent low mass sensitivity cannot be achieved. Sensitivity to below $4 M_J$ is typically not acquired, and sensitivity to $5 M_J$ planets is limited to outside $20''$ (~ 500 AU).

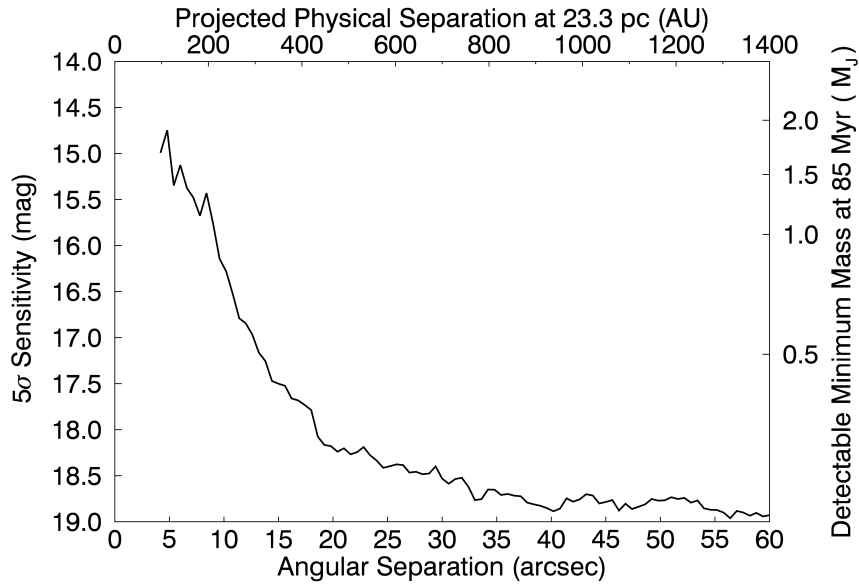


Fig. 4.— Median survey detection limits for P34 stars. Magnitude sensitivity is given as a function of angular separation. Right axis shows corresponding minimum detectable mass at median target age of 85 Myr. Top axis displays projected physical separation at median target distance 23.3 pc.

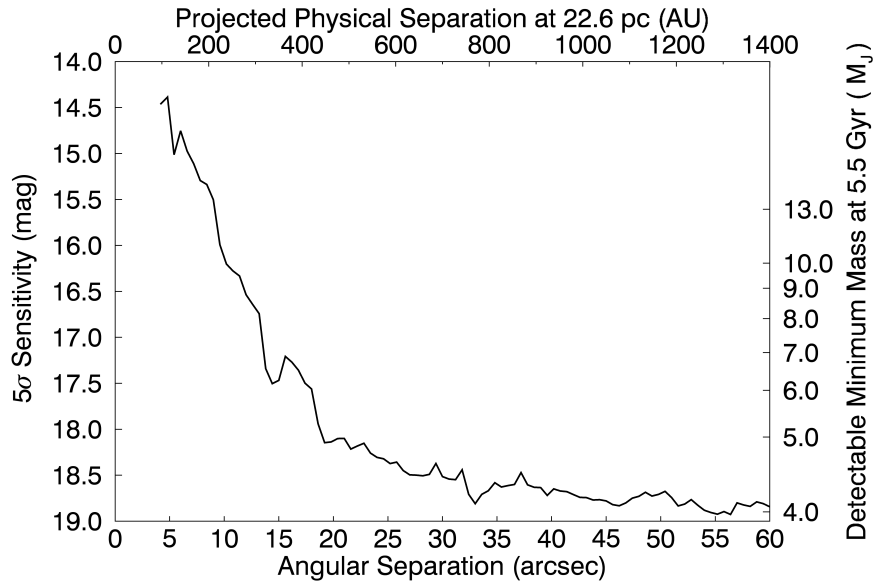


Fig. 5.— Median survey detection limits for P48 stars. Right axis shows corresponding minimum detectable mass at median target age of 5.5 Gyr. Top axis displays projected physical separation at median target distance 22.6 pc.

Taking $13 M_J$ as the upper mass limit for planetary objects, we are typically not sensitive to planets within $10''$ (~ 200 AU) for these targets.

4.2. Candidate Companion Detection

Through comparison of $3.6 \mu\text{m}$ and $4.5 \mu\text{m}$ images we initially identify 36 candidates with realistic planetary mass colour. Figure 6 shows a typical candidate identification through a $4.5 \mu\text{m}$ source non-detection at $3.6 \mu\text{m}$. These candidates are further vetted with a common proper motion analysis using a 2^{nd} epoch combining archival Spitzer data and observations carried out during Spitzer Cycle 11 under program 11102, repeating the original observations for several candidate host stars under the same observational parameters, with subsequent equivalent reduction. The target sample has a median total proper motion of 206 mas/yr , and over a baseline of 4 - 11 years provided by the 2^{nd} epoch data, we can confidently identify co-moving planetary companions in an image with a $0.6''$ /pixel scaling. Four candidates recovered in a 2^{nd} epoch are revealed to be non co-moving with the target star. Such sources are most likely rare background galaxies with unusual infrared colors, such as NGC 1377 which is brighter at $4.5 \mu\text{m}$ than $3.6 \mu\text{m}$ (Dale et al. 2005). Non-detection of the remaining sources and inspection of the raw CBCD frames leads to their identification as bad pixels surviving the Spitzer Science Center IRAC Pipeline reduction. Therefore this survey records a null planet detection result.

5. Statistical Analysis

As in previous direct imaging surveys we exploit this null detection and the magnitude detection limits generated for each target to place constraints on the wide giant population through a coupling of Monte Carlo simulations and Bayesian analysis. Effectively the Bayesian analysis determines the population of wide giants, as an upper fractional limit of stars that harbour such a companion, that is consistent with the derived planet detection probability and the null survey result. We formulate our statistical analysis in the same fashion as previous works based on Carson et al. (2006) and Lafrenière et al. (2007b). The relevance of this work is that with improved sensitivity in the PSF-noise limited regime, due to PCA application to archival Spitzer data, and the wide FOV providing background noise limited sensitivity, we have opened

sensitivity to planetary mass companions over separations on the order of $10^2 - 10^3$ AU. This has been done for both young, P34, and relatively old, P48, stars, as seen in Figures 4 and 5. With this enhanced sensitivity, we can significantly constrain the population of wide giants out to 1000 AU.

5.1. Detection Probabilities

To derive the planet detection probability for each target we simulate 10,000 planets, using a Monte Carlo approach to randomly sample planet mass, separation, orbital projection and age. Planet mass is sampled between $0.5 - 13 M_J$, however the lack of constraints on the planet population over the parameter space explored here has ensured any constraints on mass distribution are correspondingly lacking. Therefore we assume a mass distribution of $dn/dm \propto m^\alpha$ where $\alpha = -1.31$, extrapolated from statistical analysis of radial velocity studies (Cumming et al. 2008). In any case Chauvin et al. (2010) find the choice of semi-major axis power law index to dominate the derived detection probabilities in comparison to any variation in α . We choose to sample semi-major axis from a linear distribution between 100 - 1000 AU. Studies (Nielsen et al. 2008; Nielsen & Close 2010; Chauvin et al. 2010) have found semi-major axis power laws reported by Cumming et al. (2008) to be invalid at the separations considered here, motivating our choice of a linear distribution. We then sample orbital projection factor using the method of Brandeker et al. (2006) which accounts for orbital phases, orientations and an eccentricity distribution of $f(e) = 2e$ (predicted and observed for long period binaries; Duquennoy & Mayor 1991), allowing true physical separations to be translated to projected physical separations. Projected separations are then converted to angular separations using the known stellar distance. Here we do not sample over any uncertainty in stellar distance as the revised Hipparcos measurements have good precision and thus the uncertainty in stellar age completely dominates the uncertainty in detection probabilities. Age is sampled between limits of reliable estimates from the literature, or between 1 and 10 Gyr for the majority of P48 targets with ages that are not well constrained. These ages are given in Table 3. Applying COND-based evolutionary models and adopting sampled planetary properties, we can translate mass into magnitude and map each planet onto 5σ magnitude sensitivity curves. The fraction of planets that lie above the detection limit provides

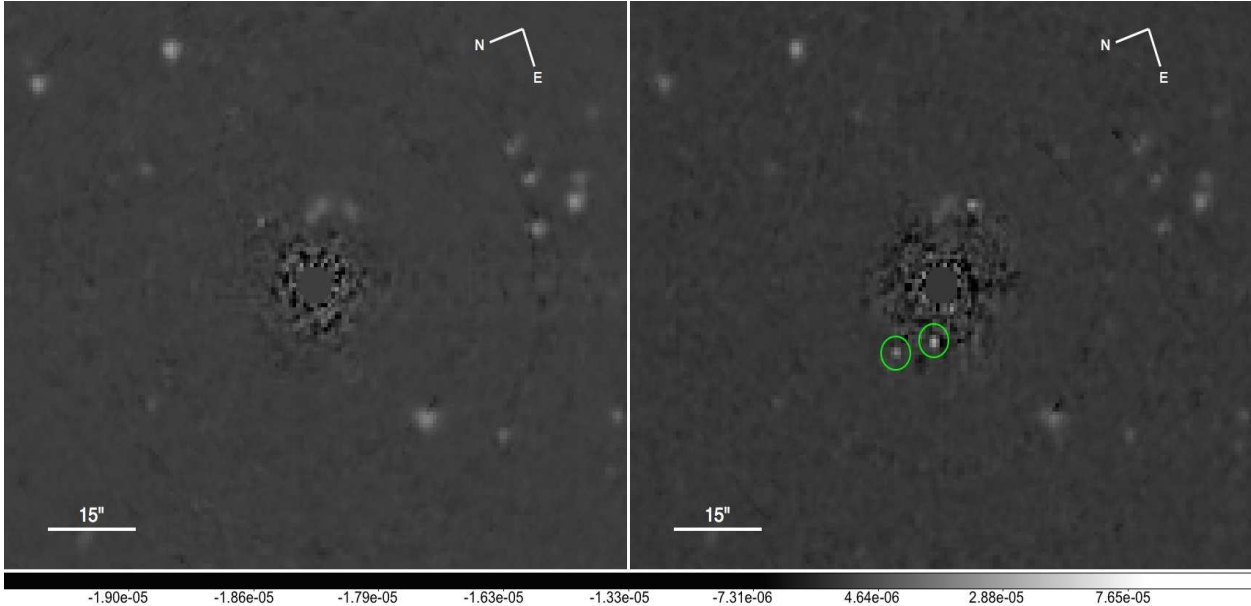


Fig. 6.— PCA reduced $3.6 \mu\text{m}$, left, and $4.5 \mu\text{m}$, right, images of HD 197890. Majority of point sources revealed appear at both wavelengths and therefore are likely background stars. Sources highlighted in green circles however only appear at $4.5 \mu\text{m}$ and are identified as potential planetary candidates. After further analysis these apparent sources were revealed to be surviving outlier pixel values.

the detection probability for each target. Mean Detection probabilities for P34 and P48 stars for mass range $[0.5, 13] M_J$ and the separation range $[100, 1000]$ AU are 0.42 and 0.08 respectively.

We additionally choose to perform simulations over varying mass and separation ranges in order to constrain the wide giant population as a function of mass and separation. Mass range will be varied between $[0.5, m_{max}] M_J$ with m_{max} ranging from 1.0 - 13.0 M_J in increments of 0.5 M_J . Separation range will be varied between $[a_{min}, a_{max}]$ with $a_{min} = 75, 100, 125$ AU, and a_{max} increasing in increments of 25 AU out to 1000 AU. Mean detection probabilities over the entire sample, as a function of upper mass and outer separation limit, are given in Figure 7. Mean detection probabilities over P34 targets are typically much greater than the mean over the entire sample due to the superior mass sensitivity of P34 targets corresponding to their relatively young ages. However we find the inclusion of P48 targets provides a favourable trade off between low probability detection and increased sample size which leads to better statistical constraints on the wide giant population.

5.2. Binary Bias

We identify 43 targets in our sample as binary stars in the Washington double star catalogue (Mason et al. 2001) that have been vetted for true companionship through a proper motion analysis. The inclusion of these binaries, $> 1/3$ of the sample, may introduce a bias in astrophysical interpretation which we attempt to account for. We recored a null planet detection in these binary systems, which is the basis of our statistical formalism. However the binary companion will have introduced a parameter space of instability in which we would not expect a planet to orbit around its host star. To deal with this and remove the bias from our analysis we use the stability criteria of Holman & Wiegert (1999) to determine the instability regions, for both S- and P-type systems. Many of the binary orbits and companion masses are not well documented, so for algorithm simplicity, consistency and to ensure conservative results, we take the worse-case scenario of an equal mass binary system, which introduces the greatest range of instability. We also assume the latest epoch separation in the Washington double star catalogue to be the true physical separation. This is a reasonable assumption as for a random distribu-

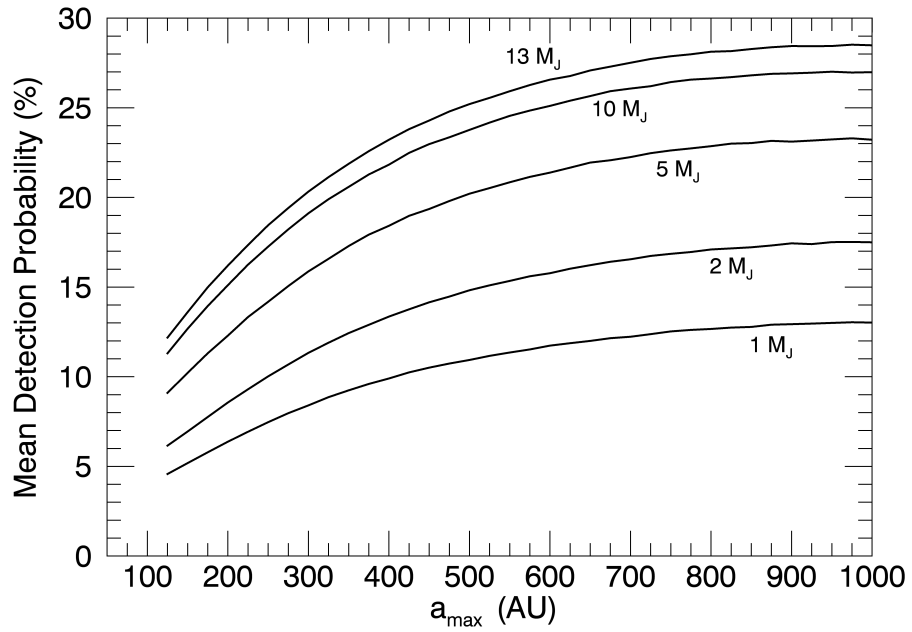


Fig. 7.— Mean planet detection probabilities over P34 and P48 targets as a function of semi-major axis and mass. X axis denotes outer limit a_{max} over which planet separation is sampled with constant $a_{min} = 100$ AU. Curves are labelled with upper mass limit m_{max} over which planet mass is sampled in units of M_J , with constant $m_{min} = 0.5M_J$.

tion of binary eccentricities, phases and orientations the most likely true physical separation is given by the projected separation (Brandeker et al. 2006). We ensure these instability regions are counted as a non-detectable range. We note that the true frequency of wide giant planets around binary stars may be different than that around single stars. This potential frequency discrepancy is possibly due to the influence that a binary companion will have on the planet formation process. Whilst studies have found that binarity has a minimal effect on overall planet frequency (Bonavita & Desidera 2007; Bergfors et al. 2013), it has been suggested that binary companions with separations $\lesssim 100$ AU may result in a decrease in the number of planets formed through enhanced dynamical heating of the protoplanetary disk (Thalmann et al. 2014). Whilst binary companions with separations $\lesssim 100$ AU only account for 12 of the 43 binaries in our sample, an element of bias will be inherent in the statistical result derived from a combined single and binary star sample.

5.3. Estimation of Planet Frequency

With the determination of target detection probabilities an upper limit on the frequency of planets hosting wide giants can be derived through the Bayesian approximation;

$$f_{max} \approx -\ln(1 - \alpha)/N\langle p_j \rangle \quad (1)$$

Where $\langle p_j \rangle$ is the mean detection probability over N targets and α is credibility level of the derived result which we choose to be 95%. We derive an upper limit on the frequency of planets in the mass range $[0.5, 13] M_J$ and the semi-major axis range $[100, 1000]$ AU to be 9%. As no previous survey has probed this parameter space to a similar degree of sensitivity there is no literature comparison to our result. However our low frequency findings certainly support the extension of previous survey findings of low frequency at separations on the order of 10 - 100 AU (see Table 1), out to 1000 AU separations, and is in general agreement with the theory of Veras et al. (2009), predicting a low frequency population of $10^2 - 10^5$ AU planets at ages > 50 Gyr. Figure 8 shows planet frequency limits as a function of mass over constant separation range 100 - 1000 AU. Figure 9 shows planet frequency as a function of separation with $a_{min} = 75, 100$ and 125 AU over constant mass range $0.5 - 13 M_J$. Whilst this study well constrains the population

of 100 - 1000 AU planets with masses ranging from $0.5 - 13 M_J$, the planet frequency upper limit increases towards smaller mass and separation limits. This is a deterioration of the population constraint due to bias inherent in the detection technique, where imaging sensitivity, and therefore detection probability, decreases with decreasing mass and separation. However, planet frequency tends to be a smoothly varying function with respect to mass and separation, and Figure 9 shows that at separations $\gtrsim 700$ AU frequency values tend to be approximately constant, corresponding to the background noise limited regime with approximately constant sensitivity. Thus there is no reason to expect that our choice of $[0.5, 13] M_J$ and $[100, 1000]$ AU boundaries are arbitrarily optimistic with regard to reasonably lower mass and separation limits.

6. Conclusions

In this paper we have presented the results of a re-analysis of two archival Spitzer imaging surveys encompassing 121 targets with varying spectral types and ages. Previously, the large PSF associated with the 0.85m Spitzer telescope diameter has severely limited its capability for directly imaging exoplanets. With the application of PCA we have removed the stellar PSF and opened up sensitivity to planetary mass companions over a broad range of separations. PCA has provided up to a magnitude sensitivity improvement at small separations with respect to conventional PSF subtraction methods, highlighting the strength of the technique, even on a relatively unfavourable data set. Using theoretical mass-luminosity evolutionary models we have shown that we are sensitive to planetary mass companions down to $0.5 M_J$ at separations on the order of $10^2 - 10^3$ AU. This parameter space has not previously been systematically explored by imaging surveys to any comparable degree of sensitivity due to anisoplanatism and FOV limitations of ground based surveys, and PSF contrast limitations of space based surveys. Therefore through the coupling of Monte Carlo simulations and a Bayesian analysis, for the first time we have constrained the population of $0.5 - 13 M_J, 100 - 1000$ AU planets, producing an upper frequency limit of 9%. This is an extension of findings of low companion frequencies in numerous previous surveys at separations on the order of $10 - 10^2$ AU. Constraining this very wide giant planet population allows for previously untested formation and evolutionary theories to be adapted and constrained.

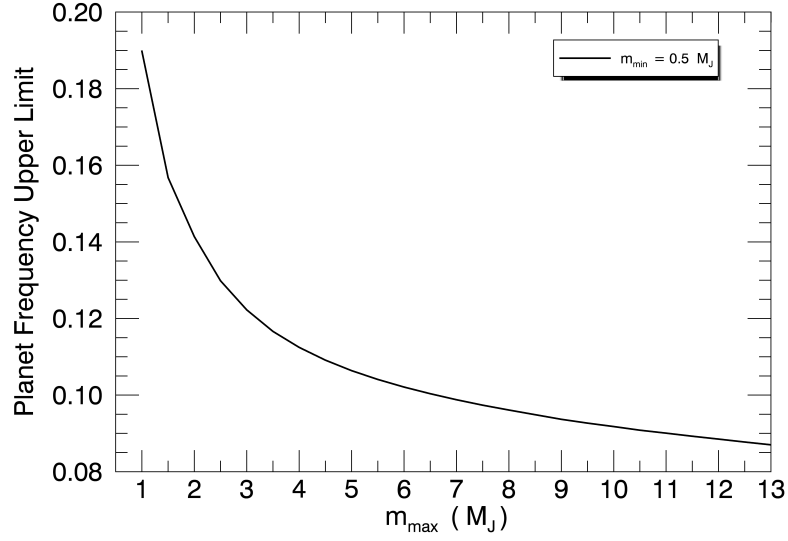


Fig. 8.— Planet frequency upper limit (at the 95% confidence level) as a function of mass. X axis denotes upper mass limit m_{max} with constant $m_{min} = 0.5M_J$. Separation range is constant, 100 - 1000 AU.

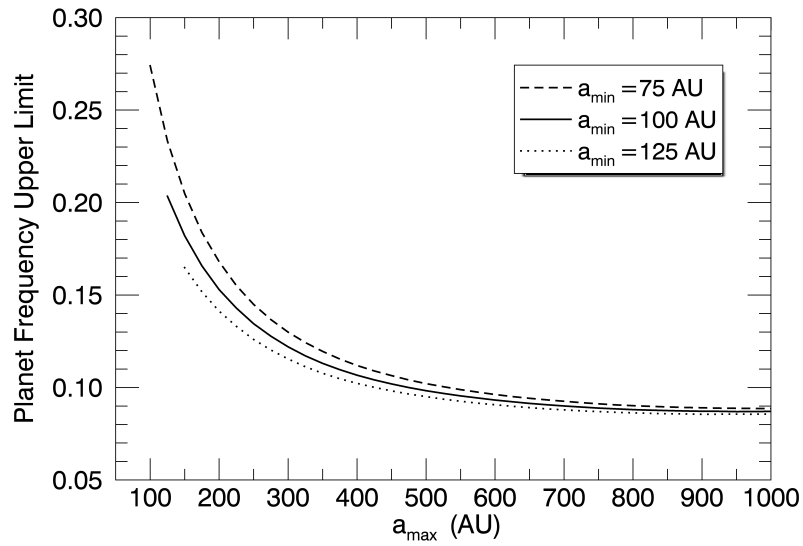


Fig. 9.— Planet frequency upper limit (at the 95% confidence level) as a function of separation. X axis denotes outer separation limit a_{max} with constant $a_{min} = 75, 100, 125$ AU. Mass range is constant, 0.5 - 13 M_J .

S.D. acknowledges support from the Queen's University Belfast Department for Education and Learning (DEL) university scholarship. M.J. gratefully acknowledges funding from the Knut and Alice Wallenberg Foundation. J.C. receives support from the Research Corporation for Science Advancement (Award No. 21026) and the South Carolina Space Grant Consortium. This work is based on observations made with the Spitzer Space Telescope, which is operated by the Jet Propulsion Laboratory, California Institute of Technology under a contract with NASA. This study made use of the CDS services SIMBAD and VizieR, as well as the SAO/NASA ADS service.

REFERENCES

- Allard, F., Hauschildt, P. H., Alexander, D. R., Tamanai, A., & Schweitzer, A. 2001, *ApJ*, 556, 357, 357
- Amara, A., & Quanz, S. P. 2012, *MNRAS*, 427, 948, 948
- Baglin, A., Auvergne, M., Barge, P., et al. 2009, in *IAU Symposium, Vol. 253, IAU Symposium*, ed. F. Pont, D. Sasselov, & M. J. Holman, 71–81
- Bailey, V., Meshkat, T., Reiter, M., et al. 2014, *ApJ*, 780, L4, L4
- Baraffe, I., Chabrier, G., Barman, T. S., Allard, F., & Hauschildt, P. H. 2003, *A&A*, 402, 701, 701
- Barnes, S. A. 2007, *ApJ*, 669, 1167, 1167
- Barrado y Navascues, D. 1998, *A&A*, 339, 831, 831
- Bergfors, C., Brandner, W., Daemgen, S., et al. 2013, *MNRAS*, 428, 182, 182
- Biller, B. A., Close, L. M., Masciadri, E., et al. 2007, *ApJS*, 173, 143, 143
- Biller, B. A., Liu, M. C., Wahhaj, Z., et al. 2013, *ApJ*, 777, 160, 160
- Bonavita, M., & Desidera, S. 2007, *A&A*, 468, 721, 721
- Boss, A. P. 2006, *ApJ*, 637, L137, L137
- Brandeker, A., Jayawardhana, R., Khavari, P., Haisch, Jr., K. E., & Mardones, D. 2006, *ApJ*, 652, 1572, 1572
- Brandt, T. D., Kuzuhara, M., McElwain, M. W., et al. 2014, *ApJ*, 786, 1, 1
- Bubenicek, J., Palous, J., & Piskunov, A. E. 1985, *Soviet Ast.*, 29, 625, 625
- Burrows, A., Sudarsky, D., & Lunine, J. I. 2003, *ApJ*, 596, 587, 587
- Butler, R. P., Marcy, G. W., Williams, E., et al. 1996, *PASP*, 108, 500, 500
- Carson, J. C., Eikenberry, S. S., Smith, J. J., & Cordes, J. M. 2006, *AJ*, 132, 1146, 1146
- Carson, J. C., Marengo, M., Patten, B. M., et al. 2011, *ApJ*, 743, 141, 141
- Chabrier, G., Baraffe, I., Allard, F., & Hauschildt, P. 2000, *ApJ*, 542, 464, 464
- Chatterjee, S., Ford, E. B., Matsumura, S., & Rasio, F. A. 2008, *ApJ*, 686, 580, 580
- Chauvin, G., Lagrange, A.-M., Bonavita, M., et al. 2010, *A&A*, 509, A52, A52
- Chauvin, G., Vigan, A., Bonnefoy, M., et al. 2015, *A&A*, 573, A127, A127
- Cumming, A., Butler, R. P., Marcy, G. W., et al. 2008, *PASP*, 120, 531, 531
- Cutri, R. M., Skrutskie, M. F., van Dyk, S., et al. 2003, *VizieR Online Data Catalog*, 2246, 0, 0
- Dale, D. A., Bendo, G. J., Engelbracht, C. W., et al. 2005, *ApJ*, 633, 857, 857
- Delorme, P., Lagrange, A. M., Chauvin, G., et al. 2012, *A&A*, 539, A72, A72
- Dodson-Robinson, S. E., Veras, D., Ford, E. B., & Beichman, C. A. 2009, *ApJ*, 707, 79, 79
- Dupuy, T. J., Liu, M. C., & Ireland, M. J. 2009, *ApJ*, 692, 729, 729
- Duquennoy, A., & Mayor, M. 1991, *A&A*, 248, 485, 485
- Ehrenreich, D., Lagrange, A.-M., Montagnier, G., et al. 2010, *A&A*, 523, A73, A73
- Eisenbeiss, T., Ammler-von Eiff, M., Roell, T., et al. 2013, *A&A*, 556, A53, A53

- Fazio, G. G., Hora, J. L., Allen, L. E., et al. 2004, *ApJS*, 154, 10, 10
- Fekel, F. C., Bopp, B. W., Africano, J. L., et al. 1986, *AJ*, 92, 1150, 1150
- Fortney, J. J., Marley, M. S., Saumon, D., & Lodders, K. 2008, *ApJ*, 683, 1104, 1104
- Fritz, T., Gillessen, S., Trippe, S., et al. 2010, *MNRAS*, 401, 1177, 1177
- Fuhrmann, K. 2004, *Astronomische Nachrichten*, 325, 3, 3
- . 2008, *MNRAS*, 384, 173, 173
- Gaidos, E. J., Henry, G. W., & Henry, S. M. 2000, *AJ*, 120, 1006, 1006
- Gliese, W., & Jahreiss, H. 1991, *NASA STI/Recon Technical Report A*, 92, 33932, 33932
- Holman, M. J., & Wiegert, P. A. 1999, *AJ*, 117, 621, 621
- Ida, S., & Lin, D. N. C. 2004, *ApJ*, 604, 388, 388
- Isella, A., Carpenter, J. M., & Sargent, A. I. 2009, *ApJ*, 701, 260, 260
- Janson, M., Bonavita, M., Klahr, H., et al. 2011, *ApJ*, 736, 89, 89
- Janson, M., Carson, J. C., Lafrenière, D., et al. 2012, *ApJ*, 747, 116, 116
- Janson, M., Quanz, S. P., Carson, J. C., et al. 2015, *A&A*, 574, A120, A120
- Jeffries, R. D., James, D. J., & Bromage, G. E. 1994, *MNRAS*, 271, 476, 476
- Jurić, M., & Tremaine, S. 2008, *ApJ*, 686, 603, 603
- Kasper, M., Apai, D., Janson, M., & Brandner, W. 2007, *A&A*, 472, 321, 321
- King, J. R., Villarreal, A. R., Soderblom, D. R., Gulliver, A. F., & Adelman, S. J. 2003, *AJ*, 125, 1980, 1980
- Koch, D. G., Borucki, W. J., Basri, G., et al. 2010, *ApJ*, 713, L79, L79
- Kraus, A. L., Ireland, M. J., Cieza, L. A., et al. 2014a, *ApJ*, 781, 20, 20
- Kraus, A. L., Shkolnik, E. L., Allers, K. N., & Liu, M. C. 2014b, *AJ*, 147, 146, 146
- Lafrenière, D., Jayawardhana, R., & van Kerkwijk, M. H. 2010, *ApJ*, 719, 497, 497
- Lafrenière, D., Marois, C., Doyon, R., Nadeau, D., & Artigau, É. 2007a, *ApJ*, 660, 770, 770
- Lafrenière, D., Doyon, R., Marois, C., et al. 2007b, *ApJ*, 670, 1367, 1367
- Lecote, J., Soummer, R., Hinkley, S., et al. 2010, *ApJ*, 716, 1551, 1551
- López-Santiago, J., Montes, D., Crespo-Chacón, I., & Fernández-Figueroa, M. J. 2006, *ApJ*, 643, 1160, 1160
- Makarov, V. V., Zacharias, N., & Hennessy, G. S. 2008, *ApJ*, 687, 566, 566
- Makarov, V. V., Zacharias, N., Hennessy, G. S., Harris, H. C., & Monet, A. K. B. 2007, *ApJ*, 668, L155, L155
- Maldonado, J., Martínez-Arnáiz, R. M., Eiroa, C., Montes, D., & Montesinos, B. 2010, *A&A*, 521, A12, A12
- Malo, L., Doyon, R., Lafrenière, D., et al. 2013, *ApJ*, 762, 88, 88
- Mamajek, E. E., & Hillenbrand, L. A. 2008, *ApJ*, 687, 1264, 1264
- Marengo, M., Megeath, S. T., Fazio, G. G., et al. 2006, *ApJ*, 647, 1437, 1437
- Marengo, M., Stapelfeldt, K., Werner, M. W., et al. 2009, *ApJ*, 700, 1647, 1647
- Marley, M. S., Fortney, J. J., Hubickyj, O., Bodenheimer, P., & Lissauer, J. J. 2007, *ApJ*, 655, 541, 541
- Masciadri, E., Mundt, R., Henning, T., Alvarez, C., & Barrado y Navascués, D. 2005, *ApJ*, 625, 1004, 1004
- Mason, B. D., Wycoff, G. L., Hartkopf, W. I., Douglas, G. G., & Worley, C. E. 2001, *AJ*, 122, 3466, 3466
- Mayor, M., Pepe, F., Queloz, D., et al. 2003, *The Messenger*, 114, 20, 20

- Montes, D., López-Santiago, J., Fernández-Figueroa, M. J., & Gálvez, M. C. 2001a, *A&A*, 379, 976, 976
- Montes, D., López-Santiago, J., Gálvez, M. C., et al. 2001b, *MNRAS*, 328, 45, 45
- Nakajima, T., & Morino, J.-I. 2012, *AJ*, 143, 2, 2
- Naud, M.-E., Artigau, É., Malo, L., et al. 2014, *ApJ*, 787, 5, 5
- Nielsen, E. L., & Close, L. M. 2010, *ApJ*, 717, 878, 878
- Nielsen, E. L., Close, L. M., Biller, B. A., Masciadri, E., & Lenzen, R. 2008, *ApJ*, 674, 466, 466
- Parker, R. J., & Quanz, S. P. 2012, *MNRAS*, 419, 2448, 2448
- Perets, H. B., & Kouwenhoven, M. B. N. 2012, *ApJ*, 750, 83, 83
- Perryman, M. A. C., Brown, A. G. A., Lebreton, Y., et al. 1998, *A&A*, 331, 81, 81
- Plavchan, P., Werner, M. W., Chen, C. H., et al. 2009, *ApJ*, 698, 1068, 1068
- Pollacco, D. L., Skillen, I., Collier Cameron, A., et al. 2006, *PASP*, 118, 1407, 1407
- Rafikov, R. R. 2007, *ApJ*, 662, 642, 642
- Rasio, F. A., & Ford, E. B. 1996, *Science*, 274, 954, 954
- Riaz, B., Gizis, J. E., & Harvin, J. 2006, *AJ*, 132, 866, 866
- Riedel, A. R., Finch, C. T., Henry, T. J., et al. 2014, *AJ*, 147, 85, 85
- Sandler, D. G., Stahl, S., Angel, J. R. P., Lloyd-Hart, M., & McCarthy, D. 1994, *Journal of the Optical Society of America A*, 11, 925, 925
- Schlieder, J. E., Lépine, S., & Simon, M. 2012, *AJ*, 143, 80, 80
- Sommer, R., Pueyo, L., & Larkin, J. 2012, *ApJ*, 755, L28, L28
- Spiegel, D. S., & Burrows, A. 2012, *ApJ*, 745, 174, 174
- Stauffer, J. R., Hartmann, L. W., Prosser, C. F., et al. 1997, *ApJ*, 479, 776, 776
- Taberero, H. M., Montes, D., & González Hernández, J. I. 2012, *A&A*, 547, A13, A13
- Tetzlaff, N., Neuhäuser, R., & Hohle, M. M. 2011, *MNRAS*, 410, 190, 190
- Thalmann, C., Desidera, S., Bonavita, M., et al. 2014, *A&A*, 572, A91, A91
- Torres, C. A. O., Quast, G. R., Melo, C. H. F., & Sterzik, M. F. 2008, *Young Nearby Loose Associations*, ed. B. Reipurth, 757
- van Leeuwen, F. 2007, *A&A*, 474, 653, 653
- Veras, D., & Armitage, P. J. 2004, *MNRAS*, 347, 613, 613
- Veras, D., Crepp, J. R., & Ford, E. B. 2009, *ApJ*, 696, 1600, 1600
- Vican, L. 2012, *AJ*, 143, 135, 135
- Vigan, A., Patience, J., Marois, C., et al. 2012, *A&A*, 544, A9, A9
- Vogt, S. S., Marcy, G. W., Butler, R. P., & Apps, K. 2000, *ApJ*, 536, 902, 902
- Werner, M. W., Roellig, T. L., Low, F. J., et al. 2004, *ApJS*, 154, 1, 1
- Wöllert, M., Brandner, W., Reffert, S., et al. 2014, *A&A*, 564, A10, A10
- Zuckerman, B., Bessell, M. S., Song, I., & Kim, S. 2006, *ApJ*, 649, L115, L115
- Zuckerman, B., Rhee, J. H., Song, I., & Bessell, M. S. 2011, *ApJ*, 732, 61, 61
- Zuckerman, B., & Song, I. 2004, *ARA&A*, 42, 685, 685
- Zuckerman, B., Song, I., & Bessell, M. S. 2004, *ApJ*, 613, L65, L65
- Zuckerman, B., Song, I., Bessell, M. S., & Webb, R. A. 2001, *ApJ*, 562, L87, L87
- Zuckerman, B., Vican, L., Song, I., & Schneider, A. 2013, *ApJ*, 778, 5, 5

TABLE 3
TARGET SAMPLE PROPERTIES

HD	HIP	Other	RA	DEC	H Mag	Spectral Type	Distance (pc)	YMG	Age (Myr)	YMG / Age Reference	Binarity
48189	31711		06 38 00.366	-61 32 00.19	4.747	G1/G2V	21.3	AB Dor	70 - 120	Z04a, M13	Y/0.6''/810''
	106231	LO Peg	21 31 01.713	+23 20 07.37	6.524	K8	24.8	AB Dor	70 - 120	Z04a, L06, M13	
113449	63742		13 03 49.655	-05 09 42.52	5.674	G5V	21.7	AB Dor	70 - 120	Z04a, N12, M13	
102647	57632		11 49 03.578	+14 34 19.41	1.925	A3Vvar	11.0	Argus	30 - 50	Z11, M13	
	23200	GJ 182	04 59 34.831	+01 47 00.68	6.450	M0Ve	25.9	β Pictoris	12 - 22	T8, S12	
174429	92680		18 53 05.875	-50 10 49.88	6.486	K0Vp	51.5	β Pictoris	12 - 22	Z04b, T8	
196982	102141		20 41 51.159	-32 26 06.83	5.201	M4Ve	10.7	β Pictoris	12 - 22	Z04b, T8	Y/2.2''
197481	102409		20 45 09.531	-31 20 27.24	4.831	M1Ve	9.9	β Pictoris	12 - 22	Z04b, T8	Y/4600''
181296	95261		19 22 51.206	-54 25 26.15	5.148	A0Vn	48.2	β Pictoris	12 - 22	Z04b, M13	Y/4.2''
	108706	GJ 4247	22 01 13.125	+28 18 24.87	7.035	M4V	8.9	Castor	100 - 300	M01b, N12	
216803	113283		22 56 24.053	-31 33 56.04	3.804	K4V	7.6	Castor	100 - 300	M01b, N12	
	114252	GJ 890	23 08 19.550	-15 24 35.80	7.301	M0Ve	22.3	Castor	100 - 300	M01b, N12	
13507	10321		02 12 55.005	+40 40 06.02	5.649	G5V	26.9	Castor	100 - 300	M01b, N12	
217107	113421		22 58 15.541	-02 23 43.38	4.765	G8IV	19.9		1000 - 10000		
206860	107350		21 44 31.329	+14 46 18.98	4.598	G0V	17.9	Her-Lyr	211 - 303	L06, F08	Y/43.2''
35296	25278		05 24 25.464	+17 23 00.72	4.029	F8V	14.4		84 - 316	B07, M08, Mk08	Y/705.2''
41700	28764		06 04 28.440	-45 02 11.77	5.149	G0IV-V	26.6	Hyades	575 - 675	M01b	
173880	92161		18 47 01.274	+18 10 53.47	4.447	A5III	28.9	Hyades	575 - 675	B85	
1237	1292		00 16 12.678	-79 51 04.24	4.990	G6V	17.5	Hyades	575 - 675	M01b	
17051	12653		02 42 33.466	-50 48 01.06	4.323	G3IV	17.2		1000 - 10000		
40979	28767		06 04 29.942	+44 15 37.59	5.509	F8	33.1		1000 - 10000		Y/192.4''
75732	43587		08 52 35.811	+28 19 50.95	4.265	G8V	12.3		1000 - 10000		Y/85.1''
120136	67275		13 47 15.743	+17 27 24.86	3.546	F7V	15.6		1000 - 10000		Y/1.8''
179949	94645		19 15 33.230	-24 10 45.67	5.101	F8V	27.6		1000 - 10000		
1835	1803		00 22 51.788	-12 12 33.97	5.035	G3V	20.9	Hyades	575 - 675	M01b, M10, N12	
222143	116613		23 37 58.488	+46 11 57.96	5.123	G3/4V	23.3	Hyades	575 - 675	M01b, M10	
108799	60994		12 30 04.774	-13 23 35.46	4.932	G1/G2V	24.7	IC2391	45 - 55	N12	Y/2.1''
30495	22263		04 47 36.291	-16 56 04.04	4.116	G3V	13.3	IC2391	45 - 55	M10	
128987	71743		14 40 31.106	-16 12 33.44	5.629	G6V	23.7	IC2391	45 - 55	M10	
19994	14954		03 12 46.437	-01 11 45.96	3.768	F8V	22.6		1000 - 10000		Y/2.1''
	117410	GJ 9839	23 48 25.691	-12 59 14.86	6.485	K5Vke	28.2	Carina	20 - 40	Z06	
27045	19990		04 17 15.662	+20 34 42.93	4.577	A3m	28.9	Octans-Near	30 - 100	Z13	
197157	102333		20 44 02.334	-51 55 15.50	3.692	A9IV	24.2	Octans-Near	30 - 100	Z13	
166	544		00 06 36.785	+29 01 17.40	4.629	K0V	13.7	Her-Lyr	211 - 303	F04, L06	
17925	13402		02 52 32.128	-12 46 10.97	4.230	K1V	10.4	LA	20 - 150	M01a, M10	
	37766	GJ 285	07 44 40.174	+03 33 08.84	6.005	M4.5Ve	6.00	LA	20 - 150	M01b	
		EY Dra	18 16 16.776	+54 10 21.62	7.960	dM1.5e	30.0 ^a	LA	20 - 150	J94	
197890	102626		20 47 45.007	-36 35 40.79	6.930	K0V	52.2	Tuc-Hor	20 - 40	K14	
10008	7576		01 37 35.466	-06 45 37.53	5.899	G5V	24.0	LA	20 - 150	M01b, M10	Y/612''
77407	44458		09 03 27.083	+37 50 27.53	5.534	G0V	30.5	LA	20 - 150	M01a, M01b	
171488	91043		18 34 20.103	+18 41 24.23	5.896	G0V	38.0	LA	20 - 150	M01b	
		V383 Lac	22 20 07.0258	+49 30 11.763	6.577	K1V	27.5 ^b	LA	20 - 150	M01a, M01b	
130322	72339		14 47 32.727	-00 16 53.32	6.315	K0V	31.7		1000 - 10000		
217014	113357		22 57 27.980	+20 46 07.79	4.234	G5V	15.6		1000 - 10000		
92945	52462		10 43 28.272	-29 03 51.43	5.770	K1V	21.4	LA	20 - 150	M01b, L06	

TABLE 3—Continued

HD	HIP	Other	RA	DEC	H Mag	Spectral Type	Distance (pc)	YMG	Age (Myr)	YMG / Age Reference	Binarity
129333	71631		14 39 00.210	+64 17 29.95	6.012	G1.5V	34.1	LA	20 - 150	M01a, M01b	Y/0.8''
181327	95270		19 22 58.943	-54 32 16.97	5.980	F5/F6V	51.8	β Pictoris	12 - 22	Z01, Z04b	
82443	46843		09 32 43.759	+26 59 18.70	5.242	G9V	17.8	Columba	20 - 40	B14	Y/64.7''
116956	65515		13 25 45.533	+56 58 13.78	5.481	G9V	21.6	Her-Lyr	211 - 303	F04, M10	
177724	93747		19 05 24.608	+13 51 48.52	3.048	A0Vn	25.5	TW Hydrae	8 - 12	N12	Y/1494.63''
29697	21818		04 41 18.856	+20 54 05.45	5.310	K3V	13.2	Ursa Major	400 - 600	M01a, M01b	
7590	5944		01 16 29.253	+42 56 21.90	5.258	G0	23.2	Ursa Major	400 - 600	F04, M10	
217813	113829		23 03 04.977	+20 55 06.87	5.232	G5V	24.7	Ursa Major	400 - 600	M01b, K03	
128311	71395		14 36 00.560	+09 44 47.46	5.303	K0	16.5		1000 - 10000		
147513	80337		16 24 01.289	-39 11 34.71	4.025	G3/G5V	12.8		1000 - 10000		Y/345''
150706	80902		16 31 17.585	+79 47 23.20	5.639	G0	28.2		1000 - 10000		
175742	92919		18 55 53.225	+23 33 23.93	5.762	K0V	21.4	Ursa Major	400 - 600	K03	
76644	44127		08 59 12.454	+48 02 30.57	2.763	A7Vn	14.5		450 - 1050	V12	Y/0.7''/2.4''
82558	46816		09 32 25.568	-11 11 04.70	5.596	K0V	18.6		50 - 75	F86, T11	
92139	51986		10 37 18.140	-48 13 32.23	3.170	F4IV	26.8		50 - 150	P09	Y/0.5''
112429	63076		12 55 28.548	+65 26 18.51	4.604	A5n	29.3		50 - 450	P09	
115383	64792		13 16 46.516	+09 25 26.96	4.107	G0V	17.6		130 - 160	M10, V12	
		GJ 3789	13 31 46.617	+29 16 36.72	7.002	M4V	7.9 ^c	Carina/Columba	20 - 40	R14	
141795	77622		15 50 48.966	+04 28 39.83	3.440	A2m	21.6		220 - 820	V12	
124498	69562		14 14 21.357	-15 21 21.76	6.781	K4V	30.2	β Pictoris	12 - 10000	C10, M13	
220182	115331		23 21 36.513	+44 05 52.38	5.574	K1V	21.5		200-318	G00, B07, M08	
20630	15457		03 19 21.696	+03 22 12.72	3.039	G5Vvar	9.14		350-700	M08, M10, V12	
130948	72567		14 50 15.811	+23 54 42.64	4.688	G2V	18.2		640-1001	D09	Y/0.1''/2.6''
142	522		00 06 19.175	-49 04 30.68	4.646	F7V	25.7		1000 - 10000		Y/4.1''
4208	3479		00 44 26.651	-26 30 56.45	6.243	G5V	32.4		1000 - 10000		
10697	8159		01 44 55.825	+20 04 59.34	4.678	G5IV	32.6		1000 - 10000		
3651	3093		00 39 21.806	+21 15 01.71	4.064	K0V	11.0		1000 - 10000		Y/42.9''
20367	15323		03 17 40.045	+31 07 37.36	5.117	F8V	26.7		1000 - 10000		
222404	116727		23 39 20.852	+77 37 56.19	1.190	K1III	14.1		1000 - 10000		Y/0.9''
27442	19921		04 16 29.029	-59 18 07.76	1.814	K2III	18.2		1000 - 10000		Y/13.1''
33636	24205		05 11 46.448	+04 24 12.73	5.633	G0	28.4		1000 - 10000		
39091	26394		05 37 09.892	-80 28 08.84	4.424	G0V	18.3		1000 - 10000		
50554	33212		06 54 42.825	+24 14 44.02	5.516	F8V	29.9		1000 - 10000		
75289	43177		08 47 40.390	-41 44 12.45	5.187	F9VFe+0.3	29.2		1000 - 10000		Y/21.5''
82943	47007		09 34 50.737	-12 07 46.37	5.245	F9VFe+0.5	27.5		1000 - 10000		
92788	52409		10 42 48.528	-02 11 01.52	5.798	G6V	35.5		1000 - 10000		
95128	53721		10 59 27.973	+40 25 48.92	3.736	G0V	14.0		1000 - 10000		
114386	64295		13 10 39.824	-35 03 17.21	6.497	K3V	28.9		1000 - 10000		
114783	64457		13 12 43.786	-02 15 54.13	5.623	K1V	20.5		1000 - 10000		
192263	99711		20 13 59.846	-00 52 00.77	5.685	K2.5V	19.3		1000 - 10000		
117176	65721		13 28 25.809	+13 46 43.64	3.457	G5V	18.0		1000 - 10000		
134987	74500		15 13 28.667	-25 18 33.65	5.121	G5V	26.2		1000 - 10000		
141937	77740		15 52 17.547	-18 26 09.84	5.866	G2/G3V	32.3		1000 - 10000		
143761	78459		16 01 02.662	+33 18 12.63	3.989	G2V	17.2		1000 - 10000		
145675	79248		16 10 24.314	+43 49 03.53	4.803	K0V	17.6		1000 - 10000		

TABLE 3—Continued

HD	HIP	Other	RA	DEC	H Mag	Spectral Type	Distance (pc)	YMG	Age (Myr)	YMG / Age Reference	Binarity
160691	86796		17 44 08.701	-51 50 02.59	3.724	G5V	15.5		1000 - 10000		
216435	113044		22 53 37.932	-48 35 53.83	4.687	G0V	32.6		1000 - 10000		
210277	109378		22 09 29.866	-07 32 55.15	4.957	G8V	21.6		1000 - 10000		
216437	113137		22 54 39.482	-70 04 25.35	4.923	G1VFe+0.3	26.8		1000 - 10000		
74575	42828		08 43 35.538	-33 11 10.99	4.227	B1.5III	269.5		13.2 - 18.4	T11	
59967	36515		07 30 42.512	-37 20 21.70	5.253	G3V	21.8	Castor	100 - 300	N12	
73350	42333		08 37 50.294	-06 48 24.78	5.318	G5V	24.0	Hyades	575 - 675	M10, T12	
37124	26381		05 37 02.486	+20 43 50.84	6.021	G4IV-V	33.7		1000 - 10000		
52265	33719		07 00 18.036	-05 22 01.78	5.033	G0V	29.0		1000 - 10000		
		AF Hor	02 41 47.31	-52 59 30.7	7.851	M2Ve	27.0 ^d	Tuc-Hor	20 - 40	M13, Z04b	Y/22.1''
36705	25647		05 28 44.830	-65 26 54.86	4.845	K0V	15.2	AB Dor	70 - 120	Z04a, L06, M13	Y/8.9''
21845	16563		03 33 13.491	+46 15 26.53	6.457	K2	34.4	AB Dor	70 - 120	Z04a, L06, M13	Y/9.6''
102077	57269		11 44 38.463	-49 25 02.75	6.642	K1V	48.6		30 - 120	W14	Y/0.2''
105963	59432		12 11 27.754	+53 25 17.45	5.867	K0V	30.2		242 - 302	B07, M08	Y/13.5''
139084	76629		15 38 57.543	-57 42 27.34	5.994	K0V	38.5	β Pictoris	12 - 22	Z04b, M13	Y/10.2''
172555	92024		18 45 26.900	-64 52 16.54	4.251	A7V	28.6	β Pictoris	12 - 22	Z04b, M13	Y/71.4''
202730	105319		21 19 51.990	-53 26 57.93	4.224	A5V	30.3		50 - 900	P09, V12	Y/7.3''
218738	114379		23 09 57.372	+47 57 30.13	5.788	G5Ve	23.7		12.7 - 48	P09, T11	Y/15.8''
51849	33560		06 58 26.051	-12 59 30.58	6.368	K4V	21.7		30 - 220	P09, T11	Y/0.7''
141272	77408		15 48 09.463	+01 34 18.27	5.610	G8V	21.3	LA	20 - 150	M01b, M10	Y/17.9''
155555	84586		17 17 25.505	-66 57 03.73	4.907	G5IV	31.5	β Pictoris	12 - 22	Z04b, M13	Y/34.04''
220140	115147		23 19 26.633	+79 00 12.67	5.512	G9V	19.2		16 - 50	Mk07, T11	Y/10.8''/962.6''
11131	8486		01 49 23.356	-10 42 12.86	5.289	G1V _k	22.6	Ursa Major	400 - 600	M01b, M10, N12	Y/192.9''
43162	29568		06 13 45.296	-23 51 42.98	4.863	G5V	16.7	IC 2391	45 - 55	M10, N12	Y/24.6''/164''
160934	86346		17 38 39.634	+61 14 16.03	6.998	K7Ve	33.1	AB Dor	70 - 120	Z04a, L06, M13	Y/0.12''
9826	7513		01 36 47.842	+41 24 19.64	2.957	F8V	13.5		1000 - 10000		Y/55.4''
13445	10138		02 10 25.934	-50 49 25.42	4.245	K0V	10.8		1000 - 10000		Y/2.4''
46375	31246		06 33 12.622	+05 27 46.53	6.072	K1IV	34.8		1000 - 10000		Y/11.2''
162020	87330		17 50 38.355	-40 19 06.07	6.649	K3V	29.4		1000 - 10000		
186427	96901		19 41 51.972	+50 31 03.08	4.695	G5V	21.2		1000 - 10000		Y/41.6''
190360	98767		20 03 37.406	+29 53 48.49	4.239	G7IV-V	15.9		1000 - 10000		Y/178.2''

NOTE.—Target right ascension (RA) and declination (DEC) values are taken from the revised Hipparcos catalogue (van Leeuwen 2007) at equinox=J2000, epoch=J2000 computed by Vizier. H band magnitudes are taken from 2MASS All-Sky Catalog of Point Sources (Cutri et al. 2003). Distances taken from revised Hipparcos catalogue unless noted otherwise with indices [a,b,c,d], relevant references given below. Column 9 notes YMG membership. Age estimates for YMG targets are taken from estimates of the group age given in table 2. Targets with unconstrained ages are assigned an age of 1 - 10 Gyr. Column 11 notes literature sources identifying YMG membership, or the sources estimating age for several young targets with no known YMG membership. Column 12 notes Y for targets identified as part of a binary system and gives the separation of the binary companion, identification and separation values are taken from the Washington double star catalogue (Mason et al. 2001).

^a(Plavchan et al. 2009)

^b(Montes et al. 2001a)

^c(Gliese & Jahreiss 1991)

^d(Riaz et al. 2006)

References. — (B07) (Barnes 2007); (B14) (Brandt et al. 2014); (B85) (Bubenicek et al. 1985); (C10) (Chauvin et al. 2010); (D09) (Dupuy et al. 2009); (F04, F08) (Fuhrmann 2004, 2008); (F86) (Fekel et al. 1986); (G00) (Gaidos et al. 2000); (J94) (Jeffries et al. 1994); (K03) (King et al. 2003); (K14) (Kraus et al. 2014b); (L06) (López-Santiago et al. 2006); (M01a, M01b) (Montes et al. 2001a,b); (M08) (Mamajek & Hillenbrand 2008); (M10) (Maldonado et al. 2010); (M13) (Malo et al. 2013); (Mk07, Mk08) (Makarov et al. 2007, 2008); (N12) (Nakajima & Morino 2012); (P09) (Plavchan et al.

2009) ; (R14) (Riedel et al. 2014); (S12) (Schlieder et al. 2012); (T8) (Torres et al. 2008); (T11) (Tetzlaff et al. 2011); (T12) (Taberno et al. 2012); (V12) (Vican 2012); (W14) (Wöllert et al. 2014); (Z01) (Zuckerman et al. 2001); (Z04a, Z04b) (Zuckerman et al. 2004; Zuckerman & Song 2004); (Z06, Z11, Z13) (Zuckerman et al. 2006, 2011, 2013).